Electronic Supplementary Information

Cucurbituril-mediated quantum dot aggregates formed by aqueous self-assembly for sensing applications

William J Peveler,*[a,b] Hui Jia,[c] Tiffany Jeen,[b] Kelly Rees,[b] Thomas J Macdonald,[d] Zhicheng Xia,[b] Weng-I Katherine Chio,[c,d,e] Suresh Moorthy,[c] Ivan P Parkin,[d] Claire J Carmalt,[d] W Russ Algar[b] and Tung-Chun Lee*[c,d]

a) Division of Biomedical Engineering, School of Engineering, University of Glasgow, Glasgow, UK, G12 8LT Email: william.peveler@glasgow.ac.uk
b) Department of Chemistry, 2036 Main Mall, University of British Columbia, Vancouver, BC, Canada, V6T 1Z1
c) Institute for Materials Discovery, University College London (UCL), UK. E-mail: tungchun.lee@ucl.ac.uk
d) Department of Chemistry, University College London (UCL), 20 Gordon Street, London, UK, WC1H 0AJ
e) Singapore Bioimaging Consortium (SBIC), Agency for Science Technology and Research (A*STAR), Singapore

Table of Contents

Materials Synthesis and Experimental Methods

All materials were purchased at reagent grade (97%) or higher purity from Sigma Aldrich, unless noted otherwise, and used as received. Water was Milli-Q 18 MΩ deionised water. Filters were Amicon Ultra centrifugal filters purchased from Merck Millipore.

Quantum dot synthesis

CdTe QDs were prepared from NaHTe, Cd(OAc)$_2$, and mercaptopropionic acid (MPA) in water in a slightly modified procedure from Tran et al.[1] Tellurium powder (26 mg, 0.2 mmol) was added to water (5 mL, degassed with N$_2$) followed by NaBH$_4$ (19 mg, 0.5 mmol), and stirred under nitrogen flow at 85 °C for 1 h until a purple/red colour developed, indicating the presence of NaHTe, and no solid Te residue could be seen.

In parallel, Cd(OAc)$_2$ (46 mg, 0.2 mmol) and MPA (30 μL, 0.34 mmol) were dissolved in degassed water (40 mL, bubbled with N$_2$) and then basified with NaOH solution (1 M) until the pH reached 12. A portion of the NaHTe solution (0.5 mL in an oxygen free syringe, accounting for needle volume) was added to the Cd/MPA solution under nitrogen atmosphere, and a colour change was immediately observed from colourless to orange. This orange solution was heated to 100 °C for 1 to 4 h, until the desired fluorescence wavelength was observed with a hand-held 365 nm lamp. Multiple batches (QD$_G$, QD$_O$, QD$_R$) were produced with distinct absorption and emission properties.

The QDs were either purified by precipitation with ethanol and resuspension in the desired volume of water, or for the NMR studies, by freeze drying a portion of the stock solution and resuspension in D$_2$O, followed by several rounds of concentration and dilution in a 30 kDa cut-off membrane filtration device. Care was taken to wash the filters prior to use with D$_2$O, to remove glycerol/azide used during storage of the devices. The final concentration of QDs was estimated from the absorbance measured at 488 nm as detailed below. As-synthesised concentrations were between 6 and 15 μM, dependent on particle size (larger, redder particles were produced at a lower concentration), and these were concentrated to between 100 and 200 μM working stock solutions.
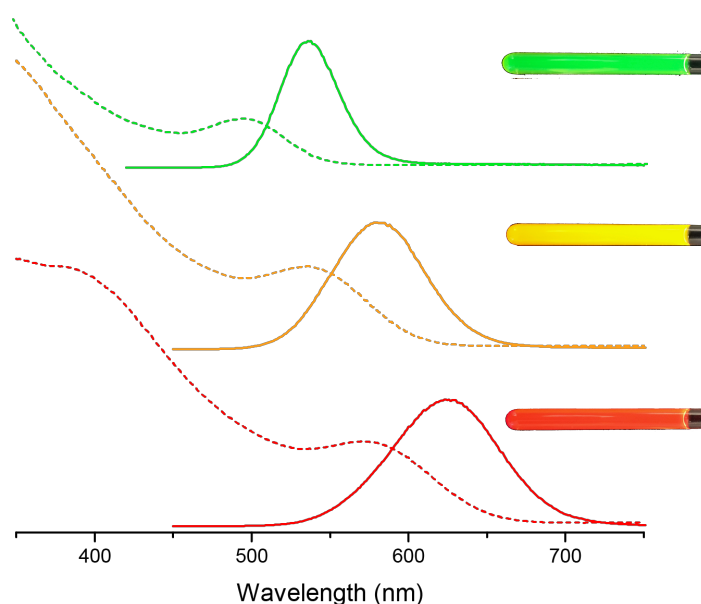
Figure S1: Normalised absorption/emission spectra for QD_G, QD_O, and QD_R with inset images showing samples under UV-illumination.

CdSe/ZnS QDs used for the comparison experiment in Figure S9 were synthesised and phase transferred from organic to aqueous solution with ligand exchange to glutathione (GSH) and MPA surface coatings using previously reported methods.[2]

Cucurbit[7]uril synthesis

Cucurbit[7]uril was purified by repeated dissolution and precipitation of a CB[5]/CB[7] mixture in weak HCl solution with MeOH, using procedures adapted from Day and Kim's groups.[3,4] The CB[7] was then deacidified using MeOH/water mixtures to precipitate and re-dissolved until neutral pH was attained. The pure CB[7] was finally dried in a vacuum oven at 60 °C for 3 days, and purity assessed by NMR and MS. ^{1}H NMR (600 MHz, D_2O): δ_H 5.73 (14H, d, J=15.3, H_{in}), 5.47 (14H, s, H_{eq}), 4.17 (14H, d, J=15.3, H_{ex}). ^{13}C NMR (150 MHz D_2O) δ_C 157.1, 69.8, 50.7. MS (ESI+ in presence of bis-imidazolium guest) m/z 733.53 ([M+BisIm]$^{2+}$ $C_{60}H_{74}N_{32}O_{14}$ calc. 733.3026).

Stock solutions of 0.1, 0.5, 2.0, 4.0 and 10.0 mM were prepared in water for QD titrations. A stock solution of 0.6 mM was prepared in D_2O for NMR studies.

QD-CB titrations

Titrations and fluorescence measurements were done in black, flat-bottomed 96 well plates at a working volume of 100 μL. Absorption measurements were done in clear bottomed half-area 96 well plates using a working volume of 100 μL. Path length in the latter case was calculated to be 0.6 cm. All liquid handling steps were done using calibrated single channel and electronic multichannel pipettes with an error of < 3 %.

In each case, aqueous CB stock solution of the appropriate concentration, and water to make up the final volume were added to the plate, before addition of appropriate volumes of QD stock solutions (aqueous) to give the final concentrations of c. 15 μM. Final QD concentration

was kept fixed wherever possible. All experiments were performed at room temperature (c. 20-23 °C) unless otherwise noted. Where imaging was required the mixed solutions were transferred to 1.5 mL Eppendorf tubes.

Nitroaromatic analyte titrations

Analyte stock solutions were prepared by mass, at highly saturated concentrations in deionised water,[5] with heating, sonication, and then cooling. These saturated solutions were allowed to settle and then in the case of DNT, used as prepared, or for NB or Toluene, diluted to the appropriate estimated concentration.

Titrations were performed using the protocol above, with the addition of the analyte. Reagents were added to the wells in the order (if used): 1) make up volume of water, 2) CB[7] stock, 3) any analyte and 4) aqueous QD stock.

Instrumental Methods

Fluorescence measurements were made on a Tecan M1000 plate reader and a Horiba Fluoromax 4 cuvette system using monochromated excitation and emission. Absorption measurements were also carried out with the Tecan M1000 system. ATR-FTIR was done on a Perkin Elmer Frontier instrument, and NMR were collected on Bruker AVANCE 600 and 400 MHz instruments. Mass spectra for Figure S12 were measured on a Waters ZQ system using positive mode electrospray ionisation (ESI) using an aqueous QD_R sample with no CB[7] present.

Proton NMR experiments were performed using a 1D NOESY sequence at a 100 ms mixing time to pre-saturate the water signal. The total delay between each scan was set to be 20 s so that data are quantitative.[6] The data were acquired with identical experimental conditions on the same day, and the accuracies of the magnitude of the signals were also validated by incorporating an synthesized electronic signal located outside the 0-10 ppm window.[7]

The Saturation Transfer Difference (STD) experiments were run with saturations alternating at 3 ppm and –100 ppm with a 50 ms Gaussian pulse train for 2 s.[8] The total relaxation delay including the saturation pulses was set to be 4 s. Long irradiation by a train of shaped low-power Gaussian pulses was selectively applied to saturate macromolecular proton NMR signals (on-resonance). All signals of the macromolecules are rapidly saturated through spin diffusion. Proton signals from the ligand bound transiently to the macromolecules also become saturated and, upon dissociation, serve to reduce the intensities of the free ligand signals. The experiment was repeated with the irradiation pulses placed outside the spectral region of macromolecule and ligand (off-resonance). The two resultant spectra were subtracted to generate the STD spectrum.

Dynamic light scattering (DLS) measurements were collected in backscatter mode on a Malvern Zetasizer Nano ZS with a 633 nm source in aqueous solution. TEM images were collected on a Jeol 2100 microscope operating at 200 kV in high-resolution mode and analysed using ImageJ. Scaled images were background subtracted, thresholded into binary colour, and ellipses were fitted. The major axis of each ellipse was used for particle sizing.

Spectrally resolved PL emission lifetime measurements were made using a custom system at LASIR, UBC Chemistry. This system consisted of an EKSPLA PL2241 pulsed picosecond laser (355 nm, 35 ps FWHM, 10 Hz repetition rate), EKSPLA Model PG401 optical parametric generator for tuneable output (420–2300 nm) and focussing optics. Detection was performed with a SP-2300i spectrograph from Princeton Instruments, with 380 nm spectral coverage and a Hamamatsu C7700 streak camera for simultaneous collection of temporal and wavelength data. Measurements were taken using 500 nm excitation, a 200 ns time window (resolution 0.4 ns), with the laser pulse at 20 ns, and spectral measurement centred on 600 nm. The excitation source was attenuated with neutral density filters to minimise pile-up at the most intense regions. Scattered light from the excitation source was visible in the spectral window measured and could be integrated to gather an in-situ measure of the instrument response function.

QD samples were prepared by mixing 3.8 nmol of QD_G and 1.8 nmol of QD_R in 200 μL of water, with or without 20 equivalents of CB (final CB[7] concentration of 0 or 0.55 mM), and measured several hours after mixing to ensure good aggregation. Data was collected to gather more than 10^5 counts at the centre of each QD emission. A spectrofluorometric plate reader measurement was made on 100 μL of each sample after lifetime measurements to verify spectral alignment and to measure absorption profiles.

Extinction measurements were performed on a home-made instrument that consisted of a 405 nm LED illuminating the sample and a photodiode placed in a transmission geometry through a 10 mm path length (2 mm path width) cuvette. A second fibre-optic was placed behind a 405 nm long pass filter at 90° to the cuvette to measure sample emission with a StellarNet Greenwave portable spectrometer. LED control and acquisition of photodiode signal and emission spectra were achieved via a custom LabVIEW program. A stable photodiode reading was obtained over c. 30 min with an aqueous QD sample (QD$_O$, 15 μM, 300 μL), and then 50 μL of concentrated CB[7] solution (4 mM in deionised water) was injected rapidly into the solution at a noted timepoint. Measurement was then continued for a further 20 min. The acquisition rate was 1 Hz.

TEM Images
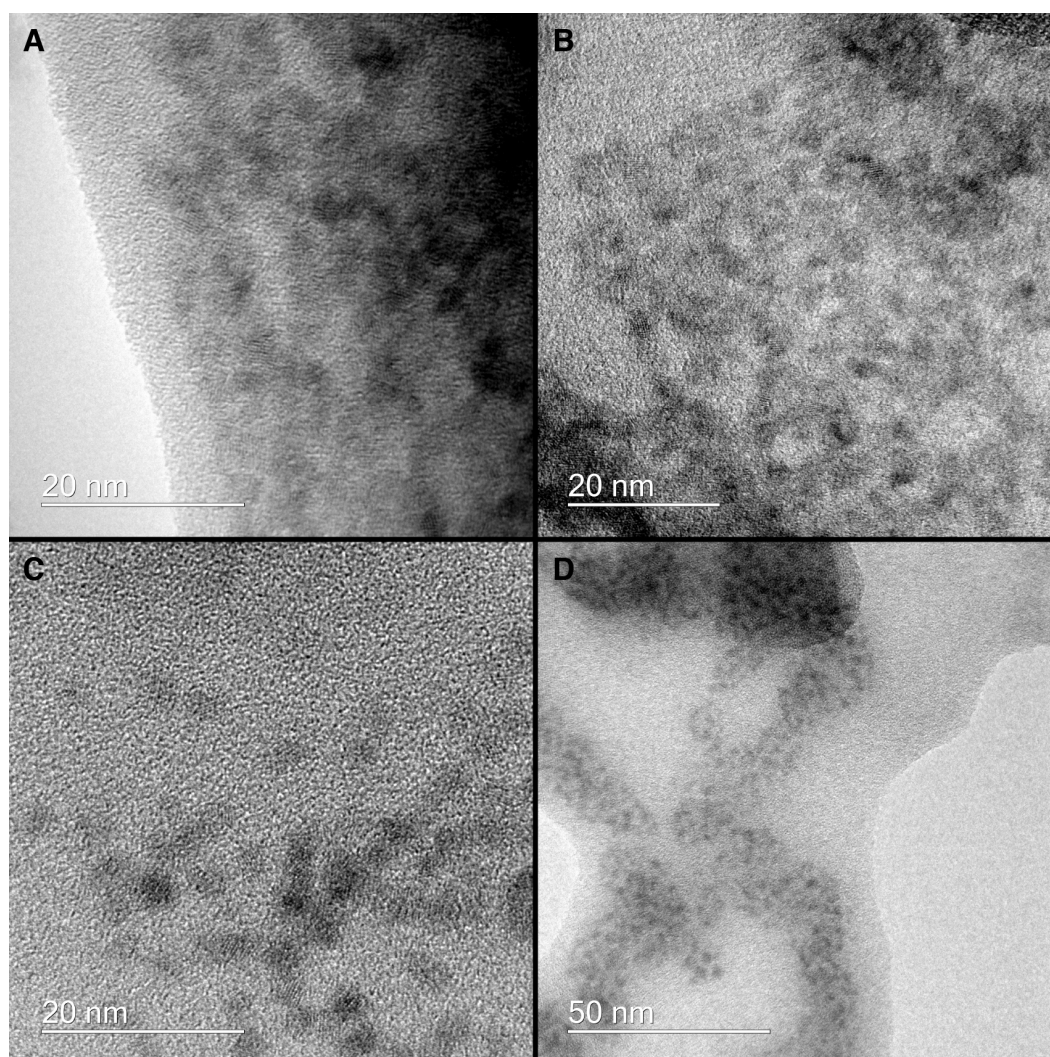
Figure S2: Sample HR-TEM images for (A) QD$_G$, (B) QD$_O$, (C) QD$_R$ without CB[7] and (D) QD$_R$ aggregated with CB[7]. Particle sizes correspond with those estimated by optical measures. Aggregation cannot be reliably assessed with TEM, as the particles will naturally aggregate as they dry on the TEM grid; however, no obvious morphological changes of the particles are observed on aggregation.

Titration spectra for CB/QD titrations with QD$_G$ and QD$_R$
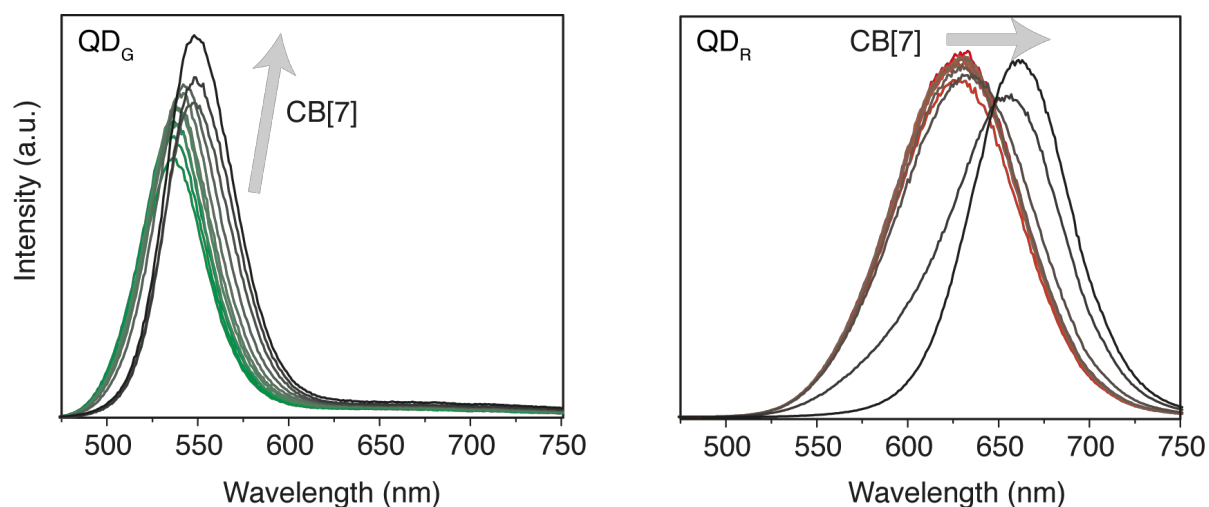
Figure S3: Titrations of 0–100 eq. of aqueous CB[7] into aqueous QD$_G$ and QD$_R$ samples at concentrations of c. 15 µM QD, 0–1.5 mM CB[7] (measured at c. 5 min after mixing).

QD Intensity change with increasing concentration of CB[7]
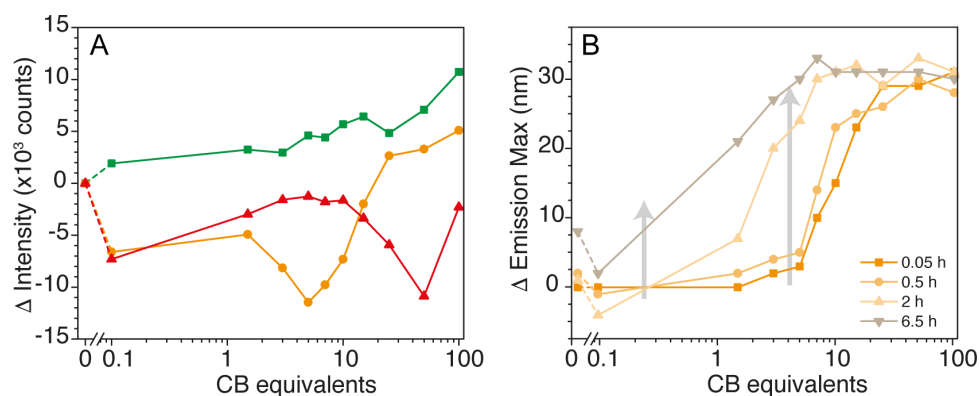
Figure S4 (A) Change in emission intensity with increasing equivalency of CB[7] measured at c. 5 mins after mixing. A characteristic dip and return is observed QD$_O$ and QD$_R$ samples but is far less pronounced for QD$_G$. (B) Change in emission maximum wavelength evolving over time with increasing CB[7] in a QD$_O$ sample. Data used in creation of Figure 1D.

Images of aggregated QD$_O$ and QD$_R$ with increasing CB[7] concentration

Figure S5: Photograph under 365 nm illumination of aqueous QD$_R$ (15 µM) aggregated with 1, 5, 10, 25 and 50 equivalents of CB[7].

Figure S6: Photograph under 365 nm illumination of aqueous QD$_O$ (15 µM) aggregated with 1, 5, 10, 25 and 50 equivalents of CB[7], showing marked precipitation for the highest concentrations after two hours.

Dynamic light scattering of QD$_G$ and QD$_O$ aggregates
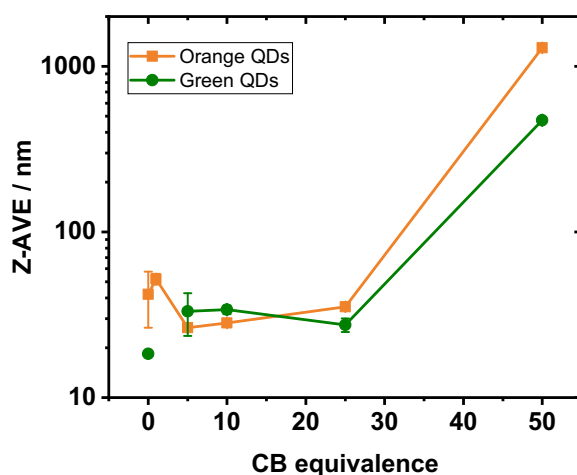
Figure S7: Data extracted from multimodal fits of dynamic light scattering data for a QD$_G$ and a QD$_O$ sample with increasing equivalencies of CB[7]. Final QD concentration in each case c. 15 μM.

Aggregated QD$_O$ sample measured with ATR-FTIR
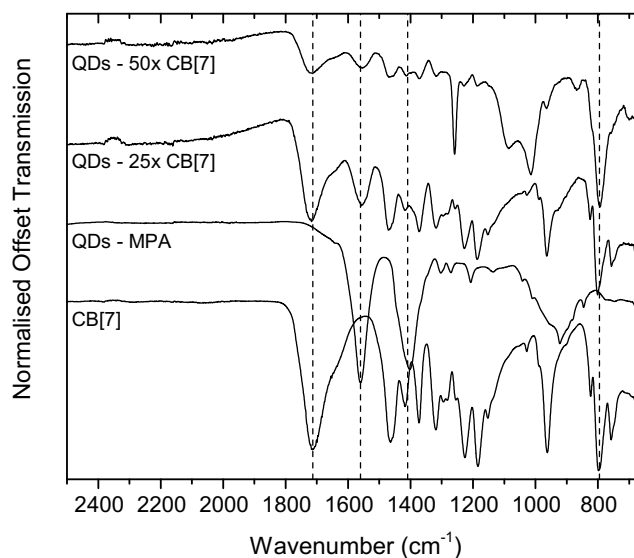
Figure S8: FTIR data for freeze-dried QD$_O$ and solid CB[7] samples, as well as aggregates of QD$_O$ produced by adding 25 or 50 eq. of CB[7] in a 0.2 mL sample of QD, and aggregating over 3 days. These samples were centrifuged to precipitate the aggregates, the supernatant was removed, and the pellet was dried under vacuum for 30 min to remove residual water before analysis. Dotted lines indicate key peaks of the CB[7] and MPA. The C=O stretch of CB[7] at 1713 cm^{-1} blue-shifts by ~10 cm^{-1} in the CB-QD aggregates and broadens slightly, suggesting qualitatively interaction between CB[7] and QDs via the electron-rich carbonyl portals of CB[7].

Calculations and assumptions for QD concentration and CB per QD values

QD concentrations were estimated using the methodology of Dong and Ren.[9] The equation:

$$\epsilon_{488\ nm} = 1745\ d^{2.66}$$

was used to estimate absorption coefficients based on estimated sizes of the QDs from their first absorption maximum (based on the method of Peng et al.[10]). TEM was measured (**Figure S2**) but accurate particle sizing was only achieved on a small number of separated particles. However, there was a reasonable correlation with the calculated sizes.

Based on the estimated QD concentrations and sizes, the following surface areas were calculated and therefore CB/nm^2 estimates could be made:

Table S1: Estimated surface coverage of QDs by CB[7]

QD	Estimated Diameter (nm)	Surface Area (nm^2)	Surface-area equivalents of CB[7] assuming close-packing		
			1 eq.	10 eq.	25 eq.
QD_G	2.3	16.6	0.12	1.21	3.02
QD_O	3.0	28.3	0.07	0.71	1.78
QD_R	3.5	38.5	0.05	0.52	1.31

Assuming close packing of CB[7] on the QD surface, the occupied surface area is 0.49 nm^2 per CB molecule. Making an assumption of spherical surface area, an approximate occupancy is calculated for various equivalencies of CB per QD. This calculation assumes favourable and reasonably permanent displacement of MPA by CB (based on slow exchange on the NMR timescale). Disregarding kinetic components, it is noticeable that, based on this model, QD_G and QD_R undergo aggregation at $t \approx 0$ min (Figure 1) when more than enough CB is present to cover the full surface. QD_O does not appear to follow this model so closely, possibly due to differing surface morphology or relative quality of MPA coverage.

Aggregation of other MPA-capped QDs
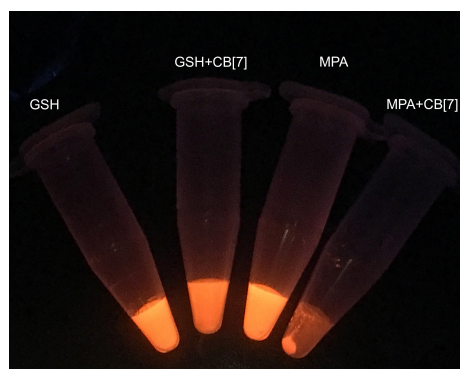
Figure S9: CdSe/ZnS QDs (final conc. c. 0.5 µM) capped with glutathione (GSH) or MPA were exposed to 50 eq. CB[7] for 30 min and then centrifuged. GSH-QDs remained largely stable to CB[7] but the MPA capped QDs were aggregated as observed with CdTe QDs. No red-shifting was observed due to the much narrower FWHM and lower polydispersity of the CdSe/ZnS QDs compared to the CdTe QDs.

1D and COSY NMR
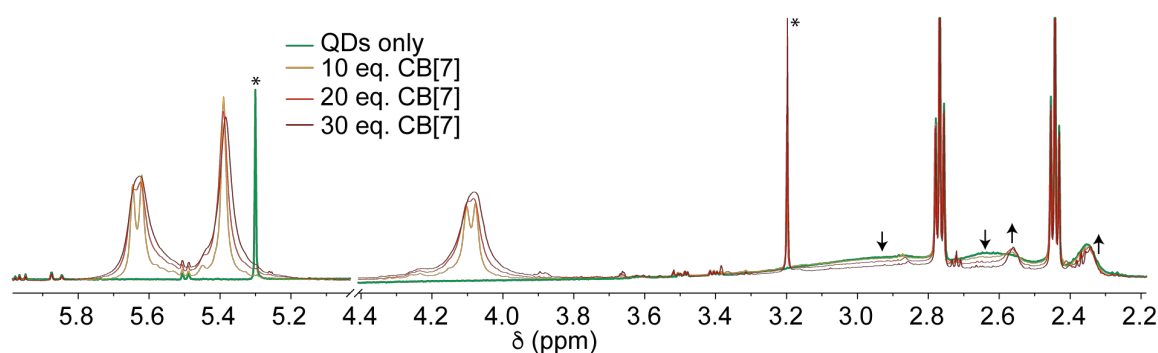
Figure S10: Full ^{1}H NMR (D$_2$O) of a QD$_R$ samples shown in Figure 2A, with MPA and CB[7] signals. Arrows indicate direction of change with increasing CB[7] concentration and * indicates solvent residues – trace DCM in QD only spectrum from NMR tube washing, and trace MeOH in all spectra from CB purification steps.
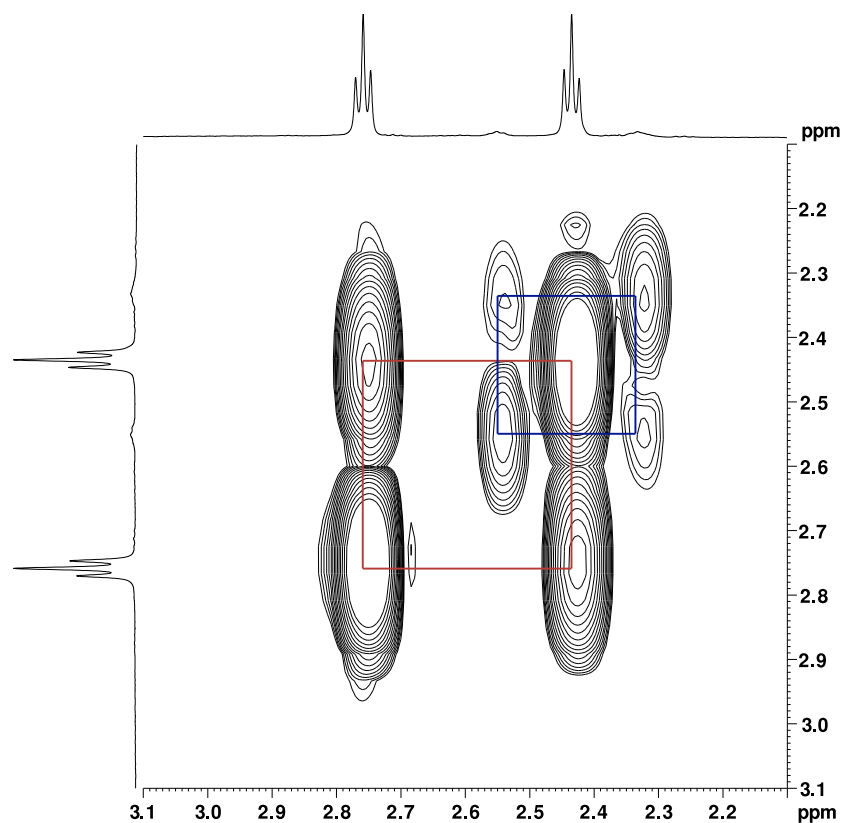
Figure S11: ^{1}H COSY NMR spectrum of the MPA region on the surface of CdTe (no CB[7] present) showing two pairs of interacting environments.

NMR and MS of disulphide side-product
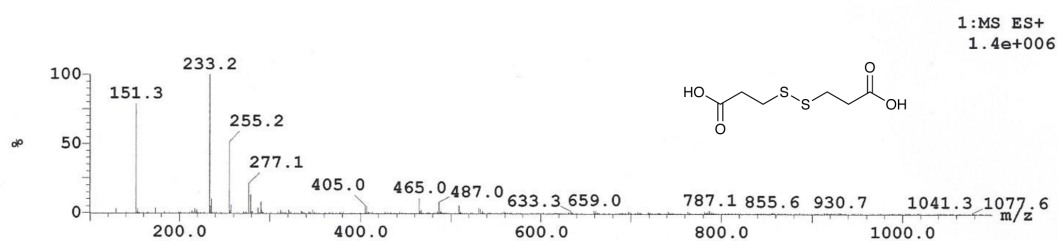
Figure S12: ESI (positive) mass spectrum of an aqueous QD_R solution confirming presence of MPA dimer: Expected mass [M] = 210, found $[M+Na]^+$ = 233, $[M+2Na-H]^+$ = 255, $[M+3Na-2H]^+$ = 277. $[MPA+2Na-H]^+$ = 151.
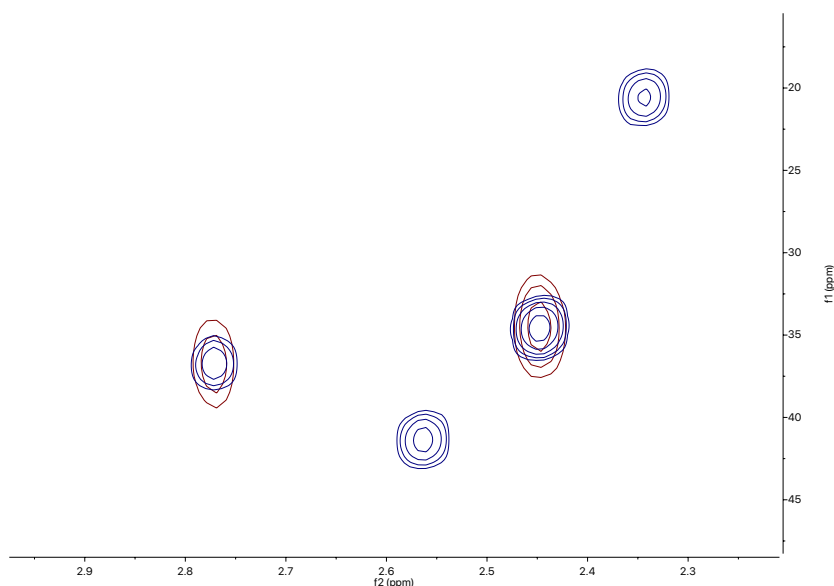
Figure S13: HMBC (^{1}H-^{13}C) 2D NMR of QD$_R$ (blue) MPA region, showing 4 major environments as per Figure 2A (main text), overlaid with a sample of MPA-dimer prepared from MPA at pH 11 (red), showing good matching.

Saturated Transfer Difference (STD) NMR
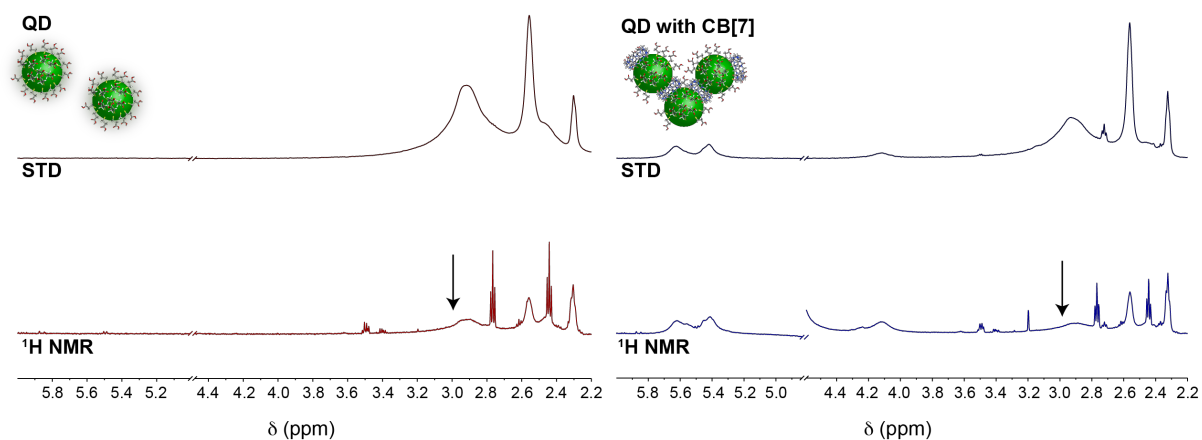
Figure S14: Saturation Transfer Difference spectra of QD$_O$ with and without 5 eq. of CB[7]. The ^{1}H NMR spectra (bottom) were saturated at both on- and off-resonance, and the difference spectra (top) only reveal the NMR signals of the bound species to the slowly rotating QD$_O$ in solution.[6] In this case, the very broad signal from the tightly bound MPA on the QD surface was irradiated at 3 ppm (indicated with an arrow), and STD data indicate, in the case of QDs alone, the other bound MPA signals (in more rapid exchange) were observed. In the case with CB[7], there was a loss in intensity for the most tightly bound MPA signals (at 2.8 and 2.4 ppm) as seen on the 1D NMR data (bottom), and CB[7] peaks were observed (4.1, 5.4 and 5.6 ppm) in the STD experiment (top), confirming their presence on the surface of the QD alongside the residual MPA.

Three-QD energy cascade
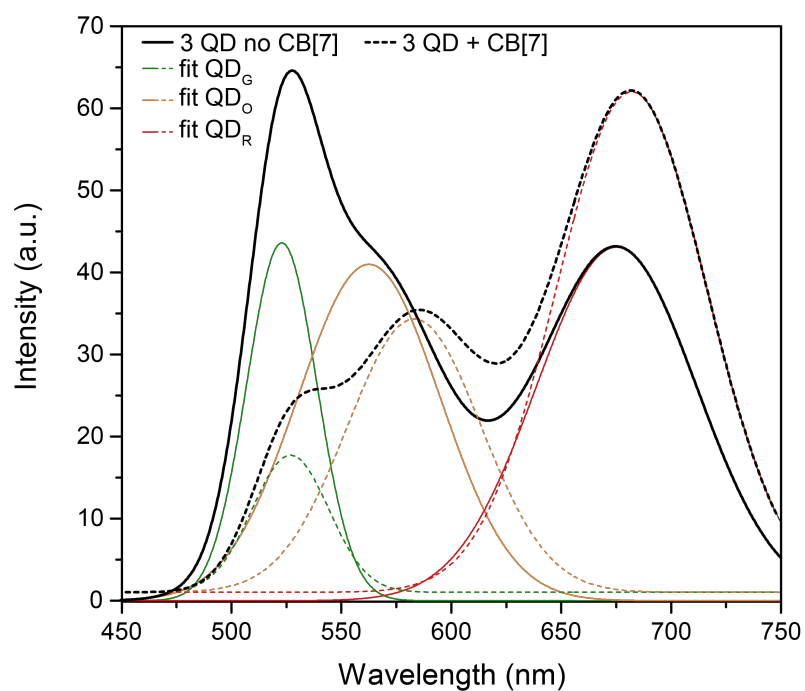
Figure S15: Emission spectra (ex. 405 nm) for three-QD mixtures with and without CB[7] aggregation in water (c. 50 eq.). Solid lines are for non-aggregated samples, dashed for the mixture with CB[7]. Multi-Gaussian peak fitting was performed to show the changes in the three components intensity and peak wavelength.

Dynamic aggregate exchange
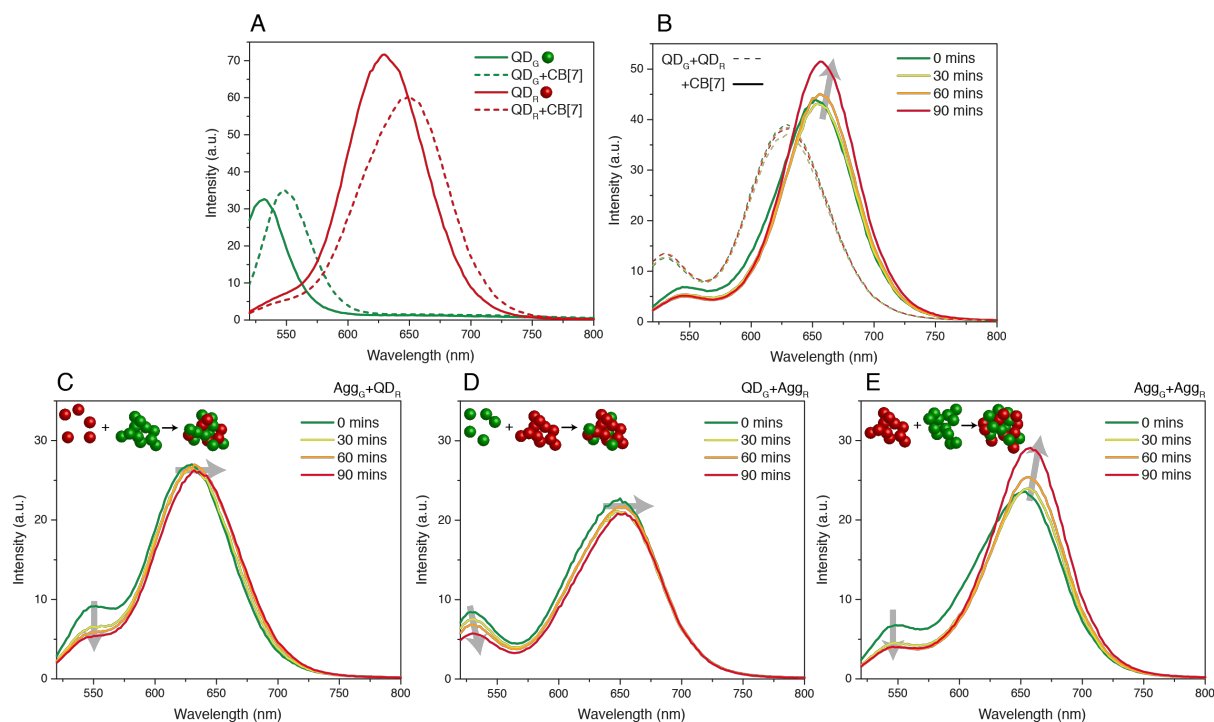
Figure S16: Exploration of the dynamic nature of the QD-CB[7] aggregates. A) c. 15 μM QD_G and QD_R solutions mixed with 10 eq. CB[7] and measured after standing for 30 min. Low equivalencies were used to ensure complete reaction between QD and CB[7] in the time period, and effects were not due to residual CB[7] B) 1:1 mixtures of QD_G and QD_R mixed at total concentration of c. 15 μM, incubated for 30 min with or without 10 eq. CB[7], then their fluorescence was measured over a further 90 min. There was very little change observed in the absence of CB[7], as expected. (C-E) 1:1 mixtures were then made of the aggregated-30-min QD/CB[7] mixtures (Agg_X) and unmodified QDs. C) Pre-aggregated green QDs mixed with QD_R show loss of green intensity and some red-shifting of the QD_R as it incorporates into the aggregates. D) When QD_G is added to pre-aggregated red QDs, the free green QD peak red-shifts as the QDs aggregate. In both cases (C&D) very little change in the red aggregate emission is seen, perhaps because full integration and energy transfer of G→R was not achieved in the measured timeframe. E) A mixture of pre-aggregated green and pre-aggregated red QDs showed the expected G→R energy transfer over 90 min, probably due to higher local CB[7] concentration (both aggregates brought CB[7] with them, rather than just one in the previous cases).

Two QD lifetime measurement tables and analysis
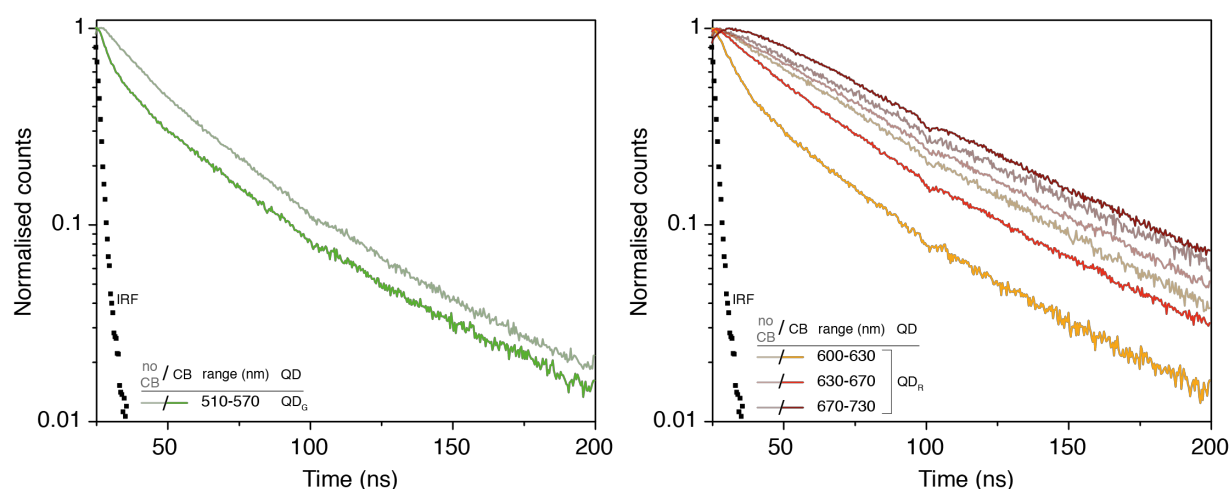
Figure S17: Normalised fluorescence decay curves for green and red components in the two-colour aggregated and non-aggregated QD mixtures excited at 500 nm. 2D plots are shown in the main manuscript. The QD$_G$ emission is integrated over the entire width (510–570 nm). The QD$_R$ signal is integrated over the blue-edge (600–630 nm), centre (630–670 nm) and red-edge (670–730 nm). The QD$_G$ gains a short component, moving from bi- to tri-exponential suggesting a fast energy transfer process on aggregation. For QD$_R$, the blue-edge and centre become bi-exponential and the shorter component is considerably reduced in length. The centre region also has a much longer component. The red-edge component lifetime remains similar but displays an increased rise-time, which is also indicative of energy transfer processes.
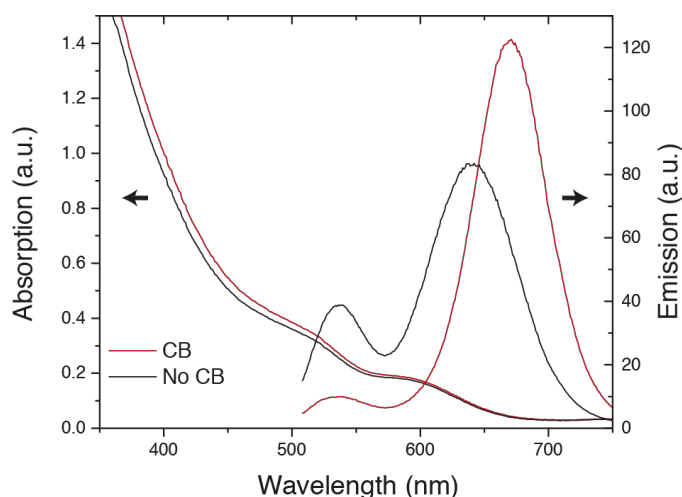
Figure S18: Emission and absorption spectra for the samples used in lifetime measurements.

Table S2: Fitted lifetimes for regions of the two-QD samples, with and without CB. Unaggregated QD data fitted with mono or bi-exponentials as suggested by Rogach et al.[11] τ_{av} is the fractionally weighted average lifetime and χ^2 is given for each fit.

	no CB				CB			
	510-570	600-630	630-670	670-730	510-570	600-630	630-670	670-730
f1	0.28	1.00	1.00	1.00	0.03	0.16	0.50	1.00
t1	18.0	47.4	52.1	57.2	2.6	7.6	30.0	56.5
f2	0.72				0.27	0.84	0.50	
t2	44.9				18.0	40.1	94.8	
f3					0.70			
t3					44.9			
τ_{av}	37.3	47.4	52.1	57.2	36.2	35.1	62.7	56.5
χ^2	1.69	1.79	2.28	1.82	2.16	1.44	1.67	2.75

Calculations of analyte/CB and analyte/QD ratios for sensing titrations
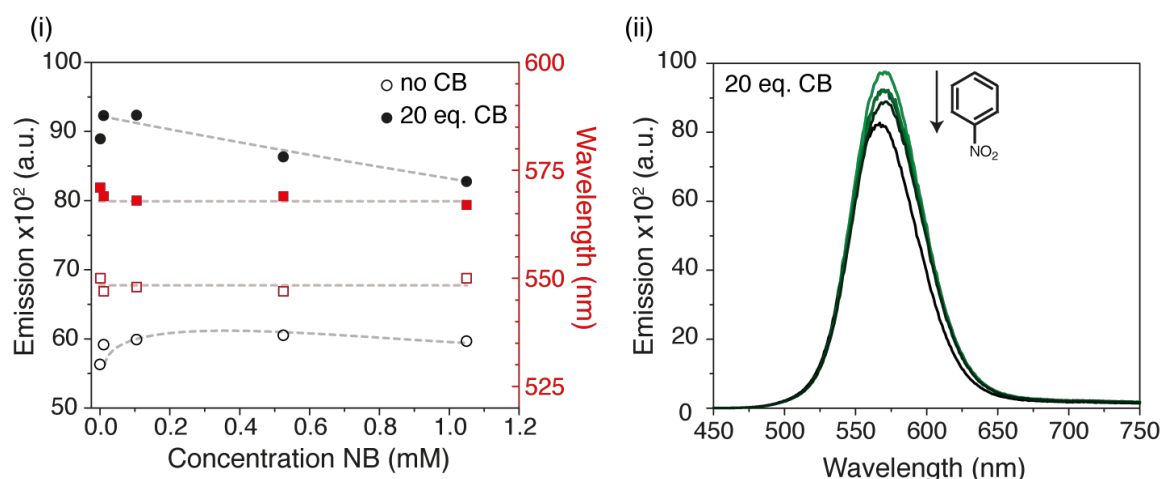
Figure S19: QD$_G$ (30 μM) with or without 20 eq. CB[7] and increasing concentrations of NB (nitrobenzene) added as a saturated aqueous solution, showing (i) a slight increase in quenching with the presence of the CB vs without and (ii) the raw fluorescence response for the "with CB" case.
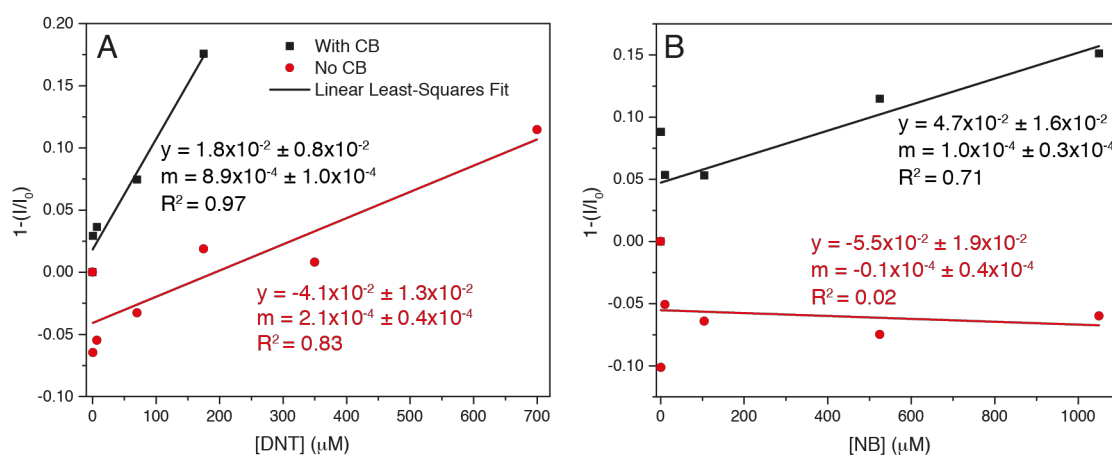
Figure S20: Linear fits of A) DNT and B) NB titrations. CB[7] appears to enhance the detection of DNT 4-fold (difference in fit gradients significant at the <0.01 level). The fit for the no-CB data is poor for the case of NB, due to the outlier data point at 1 μM, but there is a clear enhancement for NB detection with CB[7] (significant at the <0.01 level).

Table S3: For DNT detection QD concentration was c. 16 µM with 18 eq. of CB[7] in 100 µL.

Analyte Conc. (µM)	Analyte/CB[7]	Analyte/QD
0	0.000	0.00
0.7	0.002	0.04
7	0.023	0.43
70	0.233	4.26
350	1.17	21.3
700	2.33	42.6

Table S4: For NB detection QD concentration was c. 39 µM with 19 eq. of CB[7] in 100 µL.

Analyte Conc. (µM)	Analyte/CB[7]	Analyte/QD
0	0.000	0.00
1.05	0.001	0.03
10.5	0.014	0.27
105	0.140	2.72
525	0.700	13.6
1050	1.400	27.2
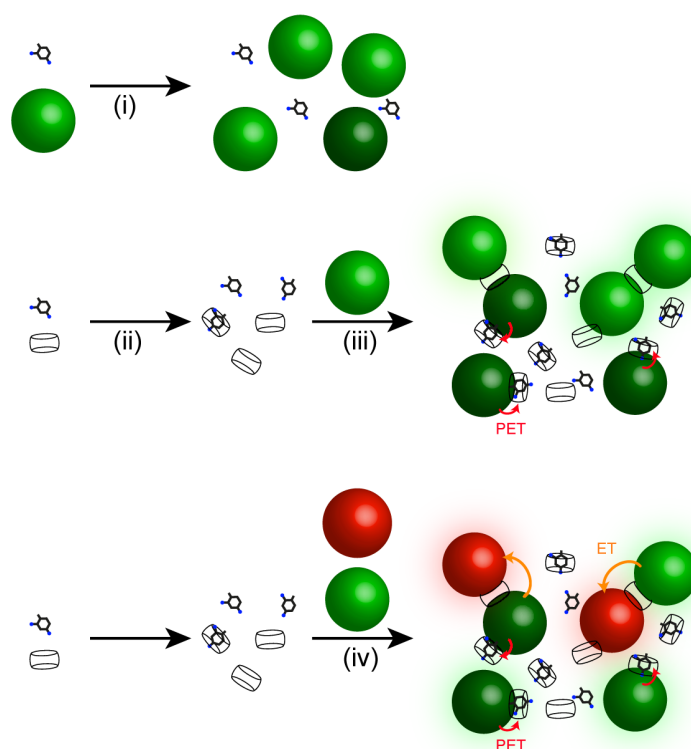
Figure S21: Schematic of QD turn-off sensing process with CB[7], expanded from **Figure 3C**. (i) QDs with DNT alone quench a little (indicated by darker shaded spheres). If CB and DNT are mixed (ii) then added to QDs (iii), aggregation (fluorescence shifting) is observed and quenching of the QDs is also increased by photoinduced energy transfer to the electron withdrawing analyte (PET – **Figure 3A**). If two colours of QDs are introduced (iv), energy transfer (ET) is observed from green to red QDs, but the process is less efficient in the presence of the analyte, suggesting some break-up of the aggregates (**Figure 3B**).

QD mixed with toluene with and without CB[7]
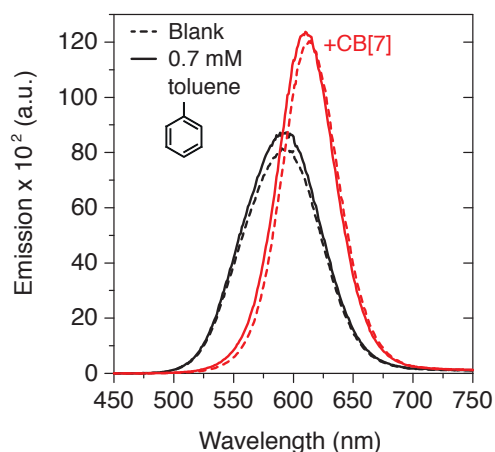
Figure S22: Emission spectra for QD$_O$ with and without 0.7 mM toluene (aqueous solution), in the presence or absence of CB[7]. Very little change is observed on analyte addition.

References

1   D. Tran, T. Macdonald, B. Wolfrum, R. Stockmann, A. Offenhäusser, T. Nann and B. Thierry, ECM-1, Basel, Switzerland, 2014, p. b001. DOI: 10.3390/ecm-1-b001

2   T. Jeen and W. R. Algar, *Bioconjugate Chem.*, 2018, **29**, 3783-3792.

3   A. Day, A. P. Arnold, R. J. Blanch and B. Snushall, *J. Org. Chem.*, 2001, **66**, 8094–8100.

4   J. Kim, I.-S. Jung, S.-Y. Kim, E. Lee, J.-K. Kang, S. Sakamoto, K. Yamaguchi and K. Kim, *J. Am. Chem. Soc.*, 2000, **122**, 540–541.

5   J. M. Phelan and J. L. Barnett, *J. Chem. Eng. Data*, 2001, **46**, 375–376.

6   E. Drijvers, J. De Roo, J. C. Martins, I. Infante and Z. Hens, *Chem. Mater.*, 2018, **30**, 1178–1186.

7   S. Akoka, L. Barantin and M. Trierweiler, *Anal. Chem.*, 1999, **71**, 2554–2557.

8   M. Mayer and B. Meyer, *Angew. Chem. Int. Ed.*, 1999, **38**, 1784–1788.

9   C. Dong and J. Ren, *Analyst*, 2010, **135**, 1395–1399.

10   W. W. Yu, L. Qu, W. Guo and X. Peng, *Chem. Mater.*, 2003, **15**, 2854–2860.

11   A. L. Rogach, T. Franzl, T. A. Klar, J. Feldmann, N. Gaponik, V. Lesnyak, A. Shavel, A. Eychmüller, Y. P. Rakovich and J. F. Donegan, *J. Phys. Chem. C*, 2007, **111**, 14628–14637.